IEEE Access
Multidisciplinary | Rapid Review | Open Access Journal

Received April 12, 2019, accepted April 19, 2019, date of publication April 30, 2019, date of current version June 3, 2019.

Digital Object Identifier 10.1109/ACCESS.2019.2914084

A Novel Wide Area Multiple Azimuth Beam ISAR Imaging System

TAOLI YANG[1], (Member, IEEE), LEI YANG[2], (Member, IEEE), GUOAN BI[3], (Senior Member, IEEE), AND YONG WANG[4]

[1]School of Resources and Environment, University of Electronic Science and Technology of China, Chengdu 611731, China
[2]Tianjin Key Laboratory For Advanced Signal Processing, Civil Aviation University of China, Tianjin 300300, China
[3]School of Electrical and Electronic Engineering, Nanyang Technological University, Singapore 639798
[4]Department of Geography, Planning, and Environment, East Carolina University, Greenville, NC 27858, USA

Corresponding author: Taoli Yang (yangtl@uestc.edu.cn)

This work was supported in part by the National Natural Science Foundation of China under Grant 61601090, Grant 41771401, and Grant 61601470, in part by the Shanghai Aerospace Science and Technology Innovation Fund under Grant SAST2016037, and in part by the Natural Science Foundation of Tianjin under Grant 20162898 and Grant 16JCYBJC41200.

ABSTRACT A novel multiple azimuth beams (MAB) inverse synthetic aperture radar (ISAR) system, as well as, the corresponding processing algorithms are proposed in this paper, which is a promising technology for wide area surveillance (WAS). This system concept is intended to obtain wide area ISAR images of multiple moving targets, which would greatly increase the surveillance velocity range compared with the single beam system. The antenna transmits a sequence of high-gain and narrow radar beams to quickly scan a wide area, and receives the echoes from all the subswaths simultaneously. Two processing methods based on digital beamforming (DBF) are presented to separate the overlapped signals for achieving the wide area ISAR images. The performance of the proposed system is analyzed from the perspectives of the surveillance area, surveillance velocity range, and steering angle error. Finally, an exemplary ISAR system is presented and verified by the simulation experiments.

INDEX TERMS Inverse synthetic aperture radar (ISAR), wide area surveillance (WAS), multiple targets imaging, multiple azimuth beam (MAB), digital beamforming (DBF).

I. INTRODUCTION

Because of the desirable superiority of target surveillance and imaging, inverse synthetic aperture radar (ISAR) has been widely used in both civilian and military applications [1], where wide area coverage is always the main capability pursued by most of the ISAR imaging systems.

There are many applications requiring wide area surveillance (WAS). For example, maritime and airspace surveillance for homeland security are desired to obtain automated surveillance capabilities to resolve and respond to any incursion in a large spatial area. In order to enlarge the surveillance area, a direct scheme has to adopt small antenna or low frequency radar to transmit a wide radar beam and simultaneously monitor multiple moving targets. There are many methods for imaging multiple moving targets within a single radar beam [2]–[7]. However, in order to distinguish different targets in one radar beam, it is required that the baseband Doppler center frequency induced by the translational velocity of the targets should be different and the difference cannot exceed the pulse repetition frequency (PRF) of the radar system [2]. Besides, if the small antenna is adopted to enlarge the surveillance area, it is hard to improve the transmitting signal power. On the other hand, if the low frequency radar is utilized, it is hard to get wideband signal yielding high range resolution images.

In order to solve the problem of single beam system, the multiple beams or multiple channel systems are studied. In [8], a multiple target imaging system is proposed. The radar system is constituted of several transceivers, which move in a fixed circular trajectory. When the targets are moving, it will be difficult to get the focused images. The similar problem is also existed in [9].

Another promising candidate for wide area imaging is using electronically scanning radars [10]–[12]. For ISAR imaging, there are mainly two kinds of operational modes,

The associate editor coordinating the review of this manuscript and approving it for publication was Mehmet Alper Uslu.

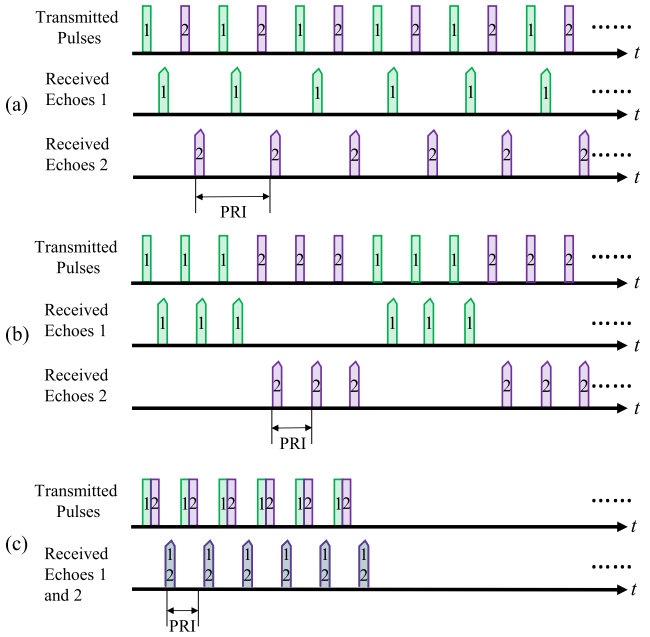

FIGURE 1. Transmitted pulses and corresponding received echoes of three operational modes: (a)uniformly sampling, (b) sparse aperture sampling, (c) the proposed sampling.

as shown in Fig. 1, where two pulses are taken as an example. One switches its line-of-sight (LOS) angle after transmitting a signal pulse and receiving the echoes. The other one switches its LOS angle after transmitting several subpulses. The pulses associated with the same indexing number, i.e., 1 or 2, represent the transmitted and received subpulses corresponding to the coverage area, or subswath. In Fig. 1(a), the equivalent PRF of received echoes is $1/N$, where N is the number of subswaths, of the transmitting PRF, which may result in lower sampling frequency than the Doppler bandwidth. In order to ameliorate this issue, sparse aperture (SA) is introduced as shown in Fig. 1(b). Compared with the uniformly sampling scheme of Fig. 1(a), the SA is discontinuous and requires a heavy computation load [13]–[15]. It should be noted that both systems immediately switch to the receiving mode after transmitting one subpulse. Thus it is hard for the system to monitor different moving targets located in different LOS area simultaneously.

In this paper, we propose a novel multiple azimuth beam (MAB) ISAR system to achieve wide area imaging, as well as a simple processing method. Although in principle, it is also a kind of electronically scanning radar, it is different from the current state-of-the-art techniques of scanning the wide area during transmission. Specifically, after continuously emitting a sequence of narrow and high-gain antenna beams to illuminate a wide area, the radar then switches to receiving mode to collect the echoes from different subswaths simultaneously, as shown in Fig. 1(c). This arrangement has three advantages as follows. The first one is that the sampling frequency for targets in each subswath would not be decreased and the sampling frequency is uniform. Therefore, it can simultaneously monitor multiple moving targets in a wide area without requiring too complex processing.[1] The second advantage is to greatly enlarge the surveillance velocity range compared with the single beam system determined by the Doppler difference induced by the translational velocity of the targets in the same radar beam. However, for our proposed system, this constraint can be relaxed by N times. Thirdly, it can monitor different moving targets located in different LOS area simultaneously. All these mentioned advantages are achieved at the processing costs for separating overlapped subpulses from different subswaths.

This paper is organized as follows. The system concept of the MAB ISAR imaging system as well as the received echo signal model are presented in Section II. Section III then introduces two methods for separating the overlapped subpulses. System performance analysis is given in Section IV. An exemplary system design and simulation experiments are given in Section V. A short summary is given in Section VI as the conclusion of this paper.

The following terms are used throughout this paper. The transmitted radar beam and pulse, illuminating a part of the wide area, are defined as subbeam and subpulse, and the corresponding illuminated area is known as subswath. Scalars, vectors, and matrices are presented by lowercase letters, bold lowercase letters, and bold uppercase letters, respectively. The superscripts T, H, -1 denote the transpose, conjugate transpose, and inverse operations, respectively.

II. SYSTEM CONCEPT

A. SYSTEM MODE

It is assumed that phased array antenna is used for the intended MAB ISAR system. The transmitters and the receivers can share the same or separated aperture. The separation of the transmitting and the receiving apertures allows to optimize the design of antennas and RF electronics for the transmitting/receiving functions at the cost of increased system complexity [16].

In this paper, the full area of antenna aperture is used for the transmitter, and is split into M independent subapertures in azimuth as receivers. The transmitting aperture size in azimuth is inversely proportional to the imaging swath width and proportional to the transmitted signal power. In order to increase the transmitted signal power, a large antenna aperture is preferred at the cost of the decreased imaging swath of one radar beam. In order to illuminate a wide area, a sequence of narrow and high-gain radar beams is transmitted to scan the designated wide area, as shown in Fig. 2, where x-axis and y-axis represent the azimuth and range directions, respectively. The relevant symbols used to define the system are listed in Table 1.

[1] Strictly speaking, it should be nearly-simultaneous since there are transmission delays among different subpulses. However, such delay, say tens of microseconds, has little effect on the moving targets and can be omitted. Therefore, the wide area surveillance can be regarded as simultaneously realized.

TABLE 1. List of symbols.

M	no. of receivers or subapertures	m	index of receiver or subapertures
N	no. of subpulses or subswaths	n	index of subpulse or subswaths
P	no. of targets	p	index of target
K	no. of scatterers	k	index of scatterer
τ	fast time	$\Delta\tau_n$	transmission delay
c	propagation velocity	r	slant range
γ	frequency modulation rate	f_c	carrier frequency
λ	wavelength	d	subaperture size in azimuth
T_{pn}	subpulse duration	B_{rn}	subpulse bandwidth
θ_{BW}	surveillance angle width	$\Delta\theta$	subbeam beamwidth
$\theta_{\{1,4\}}$	azimuth angles of beam boundaries	$\theta_{\{2,3\}}$	azimuth angles of the desired subbeam
β_n	azimuth steering angle of subbeams	α_n	azimuth angle of targets

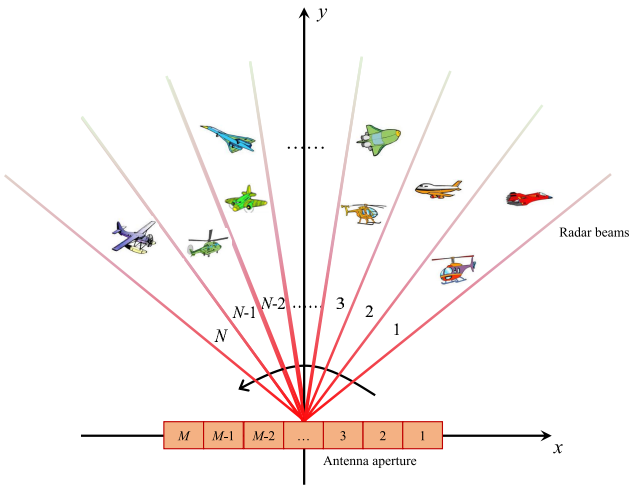

FIGURE 2. Geometry of the MAB ISAR imaging system.

The illumination sequence of the transmitted pulses can, in principle, be arranged in any order. In this paper, the order is assumed to be from the right to the left in Fig. 2. Without loss of generality, only 2-dimensional (2D) plane is considered in this paper. The radar transmits N subpulses consecutively during a pulse repetition interval (PRI) to illuminate N subswaths. In the following, let us address the subswath illuminated by the nth subpulse as the nth subswath. For enough degree of system freedom, the number of subpulses, N, should not be larger than the number of receivers, M. In fact, in order to improve the transmitted signal power and the signal processing performance, more receiving subapertures would be preferred. Nevertheless, the increase of receiving subapertures would inevitably result in higher system cost. Therefore, the number of the receiving subapertures should be determined from a proper tradeoff between the system cost and the required performance. All the transmitted subpulses are the same except that they are associated with their own steering angles in azimuth. The transmission delay between adjacent subpulses could be equal to the subpulse duration, or other suitable values as long as it is longer than the subpulse duration and satisfies the system timing requirements. Such a staggered illumination is, in some sense, similar to the traditional ScanSAR mode [17] with a major difference in receiving mode.

After transmitting N high-gain subpulses, the antenna is changed into receiving mode for all the M subapertures simultaneously receiving the echoes. As a result, the radar echoes from different subswaths are overlapped at the receiver, as shown in Fig. 1(c). More specifically, if the slant range of the target located at the first subswath is greater than the target located at the nth subswath $\frac{\Delta\tau_n \cdot c}{2}$, their echoes will overlap at the receivers if the transmission delay of the nth subpulse is $\Delta\tau_n$ compared to the first subpulse. Fortunately, the temporal overlap of the echoes from different subswaths can be solved in the spatial domain by appropriate digital beamforming (DBF) technique, which will be introduced in Section III.

It should be mentioned that the proposed SAR imaging system can also be realized by real-time beam scanning at receiver, as suggested in [16]. However, such a system has more rigorous hardware requirements because of the real-time processing. Furthermore, multiple radar beams can also be used to enlarge the elevation surveillance area. In this paper, however, we only discuss the operations in the azimuth dimension.

B. ECHO SIGNAL MODEL

Let us assume that the radar transmits linear frequency modulated (LFM) signal expressed as

$$s_{tr}(\tau) = \sum_{n=1}^{N} w_r(\tau - \Delta\tau_n) \cdot \exp\left(j2\pi f_c(\tau - \Delta\tau_n) + j\pi\gamma(\tau - \Delta\tau_n)^2\right), \quad (1)$$

where w_r is range envelope, and $\Delta\tau_n$ is the transmission delay between the nth subpulse and the first subpulse. Here, only the fast time τ, or range time, is considered in (1) for the convenience of expression since the main difference of the transmitted and received signals between the MAB system and the conventional ones is in range dimension. Furthermore, the difference of gain, i.e., Tx/Rx, due to different sub-aperture and different steering direction is neglected in this paper.

After transmitting a sequence of LFM signals, the backscattered signals from all the subswaths are received simultaneously. Ignoring the beam sidelobes and considering the additive complex white noise, the demodulated radar

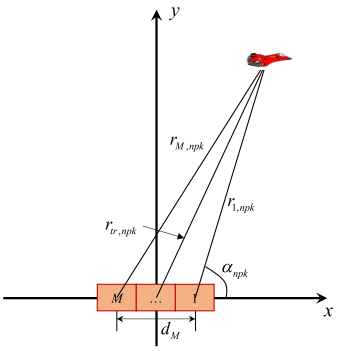

FIGURE 3. Range geometry of one target to the receivers.

signal received by the mth receiver can be modeled as

$$s_m(\tau)=\sum_{n=1}^{N}\sum_{p=1}^{P(n)}\sum_{k=1}^{K(p,n)}\sigma_{s,npk}w_r\left(\tau-\Delta\tau_n-\frac{R_{m,npk}}{c}\right)\cdot\exp\left(-j2\pi f_c\left(\Delta\tau_n+\frac{R_{m,npk}}{c}\right)\right)\cdot\exp\left(j\pi\gamma\left(\tau-\Delta\tau_n-\frac{R_{m,npk}}{c}\right)^2\right)+n_m(\tau),\quad(2)$$

where $R_{m,npk}=r_{tr,npk}+r_{m,npk}$. The point scatterer model is assumed for the targets. The number of subswaths, N, is equal to the number of the transmitted subpluses, and is smaller than the number of receivers, M. $P(n)$ represents the number of targets in the nth subswath, $K(n,p)$ is the number of the scatterers of the pth target in the nth subswath, $\sigma_{s,npk}$ is the complex reflectivity of the target, $r_{tr,npk}$ represents the range from the transmitter to the kth scatterer of the pth target in the nth subswath, $r_{m,npk}$ represents the range from the mth receiver to the kth scatterer of the pth target in the nth subswath, and $n_m(\tau)$ is the additive complex white noise with a power of σ_n^2.

Fig.3 shows the range geometry of one target in the nth subswath to the receivers. According to the imaging geometry, one can obtain

$$r_{m,npk}=\sqrt{r_{1,npk}^2+d_m^2+2r_{1,npk}d_m\cos\alpha_{npk}}\approx r_{1,npk}+d_m\cos\alpha_{npk}+\Delta r_{m,npk},\quad(3)$$

where d_m is the distance between the mth receiver to the first receiver, α_{npk} is the azimuth angle of the scatterer, $\Delta r_{m,npk}$ is the residual including the second and higher order terms. In general, $\Delta r_{m,npk}$ is small enough to allow the approximate of (3) to be

$$r_{m,npk}\approx r_{1,npk}+d_m\cos\alpha_{npk}.\quad(4)$$

Without loss of generality and for simple expression, it is assumed that there is only one target in one subswath in the following, i.e., $P(n)=1$, $n=1,\ldots,N$. It should be kept in mind that the proposed method can also handle multiple targets in one subswath. Furthermore, only one scatterer of the target is taken into consideration in the following expression, which has no advert effect on the proposed method. Therefore, (2) can be rewritten as

$$s_m(\tau)=\sum_{n=1}^{N}\sigma_{s,n}w_r\left(\tau-\Delta\tau_n-\frac{R_{1,n}+d_m\cos\alpha_n}{c}\right)\cdot\exp\left(-j2\pi f_c\left(\Delta\tau_n+\frac{R_{1,n}+d_m\cos\alpha_n}{c}\right)\right)\cdot\exp\left(j\pi\gamma\left(\tau-\Delta\tau_n-\frac{R_{1,n}+d_m\cos\alpha_n}{c}\right)^2\right)+n_m(\tau),\quad(5)$$

where $R_{1,n}=r_{tr,n}+r_{1,n}$.

Assuming that there are N targets located in N subswaths, respectively, and their range differences to the transmitter meet the condition

$$\frac{r_{tr,1}+r_{1,1}}{c}=\cdots=\Delta\tau_N+\frac{r_{tr,N}+r_{1,N}}{c}=\Delta\tau.\quad(6)$$

In such a case, the echoes from different targets in different subswaths are overlapped together. Then (5) becomes

$$s_m(\tau)=\sum_{n=1}^{N}\sigma_{s,n}w_r\left(\tau-\Delta\tau-\frac{d_m\cos\alpha_n}{c}\right)\cdot\exp\left(-j2\pi f_c\left(\Delta\tau+\frac{d_m\cos\alpha_n}{c}\right)\right)\cdot\exp\left(j\pi\gamma\left(\tau-\Delta\tau-\frac{d_m\cos\alpha_n}{c}\right)^2\right)+n_m(\tau).\quad(7)$$

III. PROCESSING ALGORITHM

Although echoes from different subswaths overlap in range at receivers, the ranges and azimuth angles of the targets differ from each other. In other words, the echoes from different subswaths are overlapped in the temporal domain but independent in the spatial domain. Therefore, the echoes from different subswaths can be distinguished using the phase differences of the overlapped signals at different receivers [18].

Since the scattered signal of a point target can occupy multiple sampling units, the range compression is needed. After the range compression, (7) becomes

$$s_{m,rc}(\tau)=\sum_{n=1}^{N}\sigma_{s,n}p_r\left(\tau-\Delta\tau-\frac{d_m\cos\alpha_n}{c}\right)\cdot\exp\left(-j2\pi f_c\Delta\tau\right)\exp\left(-j2\pi f_c\frac{d_m\cos\alpha_n}{c}\right)+n_m(\tau),\quad(8)$$

where $p_r(\tau)$ is the compressed pulse envelope. If $d_m\cos\alpha_n$ is much smaller than the range resolution which is usually

satisfied, (8) can be simplified as

$$s_{m,rc}(\tau)=\sum_{n=1}^{N} a_n(\tau)\exp\left(-j2\pi f_c\frac{d_m\cos\alpha_n}{c}\right)+n_m(\tau), \tag{9}$$

where

$$a_n(\tau)=\sigma_{s,n}p_r\left(\tau-\Delta\tau\right)\exp\left(-j2\pi f_c\Delta\tau\right). \tag{10}$$

Using vector notation, one can express the signal as

$$\boldsymbol{s}=\sum_{n=1}^{N} a_n(\tau)\boldsymbol{p}_n+\boldsymbol{n}(\tau), \tag{11}$$

where

$$\boldsymbol{s}=\left[s_{1,rc}(\tau),s_{2,rc}(\tau),\ldots,s_{M,rc}(\tau)\right]^T_{M\times 1}, \tag{12}$$

$$\boldsymbol{p}_n=\left[1,\ldots,\exp\left(-j2\pi f_c\frac{d_M\cos\alpha_n}{c}\right)\right]^T_{M\times 1}, \tag{13}$$

$$\boldsymbol{n}(\tau)=[n_1(\tau),n_2(\tau),\ldots,n_M(\tau)]^T_{M\times 1}. \tag{14}$$

The problem presented in (11) can be solved by a variety of array signal processing methods. In this paper, we propose two methods to separate the overlapped subpluses. Method I is based on the standard beamforming that always has analytical solution with rigid system requirements [19]. Method II obtains the optimal solution by minimizing the mean-square error between the array response and the desired response over a mainlobe region subject to a mean-square sidelobe constraint [20].

A. METHOD I

Assuming the weight vector is $\boldsymbol{\omega}$, the output signal power is

$$\begin{aligned}G(\tau)&=\|\boldsymbol{\omega}^H\boldsymbol{s}(\tau)\|_2^2\\&=\boldsymbol{\omega}^H\boldsymbol{s}(\tau)\boldsymbol{s}^H(\tau)\boldsymbol{\omega}\\&=\boldsymbol{\omega}^H\boldsymbol{R}_s(\tau)\boldsymbol{\omega},\end{aligned} \tag{15}$$

where

$$\boldsymbol{R}_s(\tau)=\sum_{n=1}^{N} a_n^2(\tau)\boldsymbol{p}_n\boldsymbol{p}_n^H+\sigma_n^2\boldsymbol{I}, \tag{16}$$

is the $M\times M$ covariance matrix corresponding to the array output from the range bin τ, and $\boldsymbol{I}$ is an identity matrix. According to the minimum noise variance algorithm, the weight vector can be obtained by solving the following constrained optimization problem [19], [21]:

$$\begin{cases}\text{minimize} & \boldsymbol{\omega}^H\boldsymbol{R}_s(\tau)\boldsymbol{\omega}\\ \text{subject to} & \boldsymbol{\omega}^H\boldsymbol{P}=\boldsymbol{e}\end{cases} \tag{17}$$

where

$$\boldsymbol{P}=[\boldsymbol{p}_1,\ldots,\boldsymbol{p}_N], \tag{18}$$

and $\boldsymbol{e}$ is a unity vector basis determined by the interested target direction. If the interested target is $a_1(\tau)$, then $\boldsymbol{e}=[1,0,\ldots,0]^T$. Such a constraint not only retains the interested target, but also forms deep notches in the directions of the interference signals from other subswaths. The optimal solution to the optimization problem in (17) is

$$\boldsymbol{\omega}(\tau)=\frac{\boldsymbol{R}_s^{-1}(\tau)\boldsymbol{P}\boldsymbol{e}}{\boldsymbol{P}^H\boldsymbol{R}_s^{-1}(\tau)\boldsymbol{P}}. \tag{19}$$

It should be noted that (17) restricts only signals from N different discrete angles, i.e., Method I treats the targets as point-like targets.

By changing the direction of $\boldsymbol{e}$, the overlapped echoes from different subswaths can be separated from each other. Then the phase term of each echo due to the transmission delay can be compensated by

$$\begin{aligned}&a_n\left(\tau\right)\exp\left(j2\pi f_c\Delta\tau_n\right)\\&\quad=\sigma_n p_r\left(\tau-\Delta\tau_n\right)\exp\left(-j2\pi\frac{f_c}{c}\left(r_{1,n}+r_{tr,n}\right)\right)\end{aligned} \tag{20}$$

After separating the subpluses, multiple moving targets and high resolution imaging methods can be applied to each subswath signal to obtain the wide area multiple moving targets images [2], [14].

In practice, the statistical covariance matrix $\boldsymbol{R}_s(\tau)$ can be estimated by the sample covariance matrix, or be approximated as

$$\hat{\boldsymbol{R}}_s=\sum_{n=1}^{N}\boldsymbol{p}_n\boldsymbol{p}_n^H, \tag{21}$$

if the azimuth angle α_n of the target is known. Because α_n is unknown in most cases, it is replaced by the subbeam azimuth steering angle β_n.

B. METHOD II

In Method I, the target's azimuth angle α_n is replaced by the subbeam azimuth steering angle β_n to estimate the covariance matrix, which would inevitably induce the steering error and yield decreased performance. Furthermore, even if the target is exactly located at the subbeam center, the beamforming performed by Method I is perfect only for the scatterers located in the steering direction of the subbeam center. For other scatterers not located in the direction of the subbeam center, i.e., those from large size targets in azimuth, the weight vector cannot separate them from other targets and has residual ambiguities. Therefore, Method I is only suitable for relatively small targets located at the subbeam centers.

In order to overcome the limitations of Method I, we propose a novel beamforming method, named as Method II. In fact, when separating different subpulses, there is no need to form nulls in the directions of the interferences. Let us treat the desired target as signal, and the others as the interferences. Both the desired targets and the interferences come from a known angle range determined by the transmitting beamwidth and the steering angle. For example, to extract the target from subswath 2, as shown in Fig. 7, we can treat all the echoes coming from the angle range [88.85 °, 91.15 °] as the desired signals. Those coming from the angle ranges

[86.56 °, 88.85 °] and [91.15 °, 93.44 °] are considered as interferences. Therefore, the directional pattern should retain the power in the desired angle range, i.e., the mainlobe, and suppress the interferences from other angle ranges. The requirement can be reformatted as the following constrained optimization problem [20]:

$$\begin{cases} \text{minimize} & \left(\boldsymbol{\omega}-\boldsymbol{p}_{n_0}\right)^H \boldsymbol{R}_0 \left(\boldsymbol{\omega}-\boldsymbol{p}_{n_0}\right) \\ \text{subject to} & \boldsymbol{\omega}^H \boldsymbol{R}_1 \boldsymbol{\omega} \le \xi \end{cases} \tag{22}$$

where $\boldsymbol{p}_{n_0}$ is the steering vector of the desired target or the mainlobe,

$$\boldsymbol{R}_0 = \int_{\theta_2}^{\theta_3} \boldsymbol{p}(\theta)\boldsymbol{p}^H(\theta)d\theta, \tag{23}$$

$$\boldsymbol{R}_1 = \int_{\theta_1}^{\theta_2} \boldsymbol{p}(\theta)\boldsymbol{p}^H(\theta)d\theta + \int_{\theta_3}^{\theta_4} \boldsymbol{p}(\theta)\boldsymbol{p}^H(\theta)d\theta, \tag{24}$$

where θ_1 and θ_4 represent the azimuth angles of the transmitted beam boundaries as shown in Fig. 7, $\theta_2 = \beta_{n_0} - \frac{\Delta\theta}{2}$, $\theta_3 = \beta_{n_0} + \frac{\Delta\theta}{2}$, β_{n_0} is the subbeam steering angle of the desired subpulse and ξ is the mean-square sidelobe level. Because both $\boldsymbol{R}_0$ and $\boldsymbol{R}_1$ are symmetric positive definite matrices, the problem in (22) is therefore a convex optimization problem. Specially, it is a quadratically constrained quadratic program (QCQP) that can always be efficiently solved with an optimal solution [22].

It should be noted that both processing methods are independent of the received data, since the covariance matrices are obtained according to the known system parameters as shown in (21), (23) and (24). In other words, the performance of the methods remains unchanged no matter what the noise level is.

In practice, when the imaging system is determined, it only needs to solve the problem in (17) or (22) for N times, and then store the results for all the data acquired with the predetermined illumination geometry. For Method I, the main computational load is for the matrix inversion which requires a computational complexity in the order of $O(M^3)$. For Method II, the weight vector can be directly solved by using some iterative methods, which require an $M \times M$ matrix inversion for each iteration. Usually, after several iterations, the optimal solution can be obtained. The computational time of the two methods is given in Section V.

C. PROCESSING PROCEDURES

According to the proposed method, the block diagram of the procedures is shown in Fig. 4. The processing steps are described as follows.

Range Compression: performing range compression to the received echo from each subaperture and obtaining $s_{m,rc}(\tau)$.

Weight Vector Calculation: calculating the weight vectors for the corresponding subpulses according to (19) or (22). In practice, this step can be performed in advance, and the obtained results are used as input parameters.

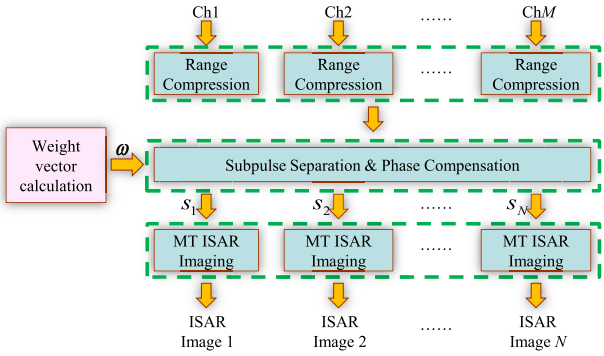

FIGURE 4. Flowchart of wide area MAB ISAR imaging.

Subpulse Separation and Phase Compensation: according to the weight vector $\boldsymbol{\omega}_1, \boldsymbol{\omega}_2, \ldots, \boldsymbol{\omega}_N$, the overlapped subpulses can be separated for ISAR imaging. Since the subpulses are transmitted in sequence, there are constant phase differences due to the time delay between echoes received from different subswaths. In practice, the phase difference can be compensated by adding a constant phase related to the transmission delay.

Multiple Targets ISAR Processing: the separated subpulses are processed by utilizing available multiple targets (MT) ISAR imaging operations to achieve the ISAR images of multiple targets ISAR images.

IV. PERFORMANCE ANALYSIS

In this section, the system performance is studied in terms of a few primary parameters of the proposed MAB ISAR system.

A. SURVEILLANCE AREA

Since the MAB ISAR system transmits N subbeams during a PRI, its surveillance area can be theoretically N times of that supported by the single beam system. Fig. 5 shows an example of three subbeams, and each with a surveillance range of 1.5 km. With the transmission delay of 10 μs between adjacent subpulses, the range difference is 1.5 km. The whole area is divided into subswath 1, subswath 2 and subswath 3. These three subbeams cover an area that is three times of that of the single beam in cross-range dimension. However, the surveillance area in range is not continuous because of the transmission delay and the sampling scheme, as shown in Fig. 5(a), in which the illumination sequence is in an anti-clock direction. In order to continuously cover the whole area, we can adopt a staggered transmitting scheme. Let us take an example of three subbeams, Tr1, Tr2 and Tr3, transmitted during a PRI. We use the expression of (Tr2, Tr1, Tr3) to represent the sequence order of subswath 2, subswath 1, and subswath 3. With proper arrangements, the entire surveillance area can be covered by the three subbeams. In this example, (Tr1, Tr2, Tr3), (Tr2, Tr3, Tr1) and (Tr3, Tr1, Tr2) are the alternative transmitting schemes, as shown in Fig. 5(b) in which the same shading pattern indicates the illumination areas covered by the same transmitting scheme.

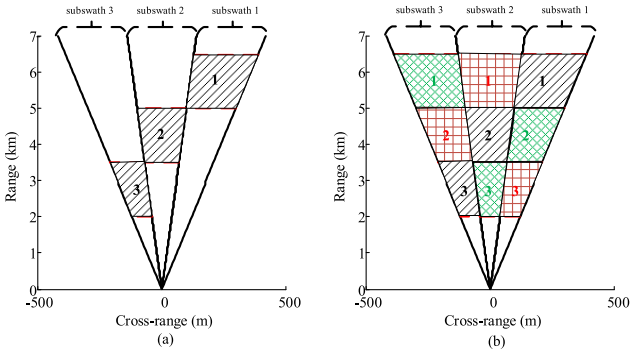

FIGURE 5. Surveillance area of the MAB ISAR system with one (a) and three (b) kinds of transmitting schemes.

B. SURVEILLANCE VELOCITY RANGE

Let us consider the case that there are multiple targets in the beam and their ranges to radar are the same. In order to distinguish them in azimuth by the single beam ISAR system, their maximum baseband Doppler center frequency difference induced by the translational motion should not exceed PRF [2], i.e.,

$$\left|\text{Frac}\left(\frac{2v_1/\lambda}{\text{PRF}}\right) - \text{Frac}\left(\frac{2v_2/\lambda}{\text{PRF}}\right)\right| < 1, \qquad (25)$$

where Frac extracts the fraction of the argument, v_1 and v_2 represent the translational velocities of the moving targets in the same beam. Otherwise, there will be problems of overlapping with other targets and image defocusing.

With the proposed MAB ISAR system, the subbeams and the staggered illumination strategy make it possible to distinguish multiple targets with much larger differences of translational velocity. Although the constraint in (25) still holds for each subbeam, however, such a requirement is not needed for targets in different subbeams. Therefore the detected translational velocity range is about N times of that in the single beam system.

C. STEERING ANGLE ERROR

According to the optimization problems shown in (17) and (22), it is seen that both processing methods presented in Section III have assumed that the steering angle of the interested target is known, although Method II does not have such a requirement for the interferences. In fact, however, there is no information on the directions of the targets exactly. Usually, the targets also span certain angular interval along the cross-range rather than a certain angle. Furthermore, for a target with certain size, the lower its altitude is, the wider angle range it would occupy. For example, if the size of a target in azimuth is 40 m, its angle range is about 0.23 ° when the slant range is 10 km, and its angle range is increased to 1.45 ° when the slant range is 2 km. Fortunately, although the targets' directions are unknown, the angle range can be determined by the direction of the transmitted beam and its beamwidth.

In Method I, the direction of the target α_n is assumed to be the direction of the subbeam β_n. However, even if the target center is perfectly located in the direction of the transmitted beam, there is still steering angle error for the scatterers deviated from the beam center. Such a problem becomes worse for targets of lower altitude. The deviation of the steering angles would inevitably decrease the interested target gain, while increasing the gain of the interference, which results in the deteriorated signal to interference ratio (SIR). In Method II, although the effect of the steering angle error on the interference suppression is controlled, the decrease of the signal gain is unavoidable. Therefore, the deviation of the steering angle error will deteriorate the SIR for both methods.

Fig. 6 shows the variation of SIR with the steering angle error obtained from a simulation whose system parameters are listed in Table 2. The blue solid and red dashed lines represent the results of Method I and Method II, respectively. The numbers of the subbeams are from $N = 2$ to $N = 7$, and the number of the receivers is $M = 8$. It is seen that Method I can achieve great SIR if there is no steering angle error.

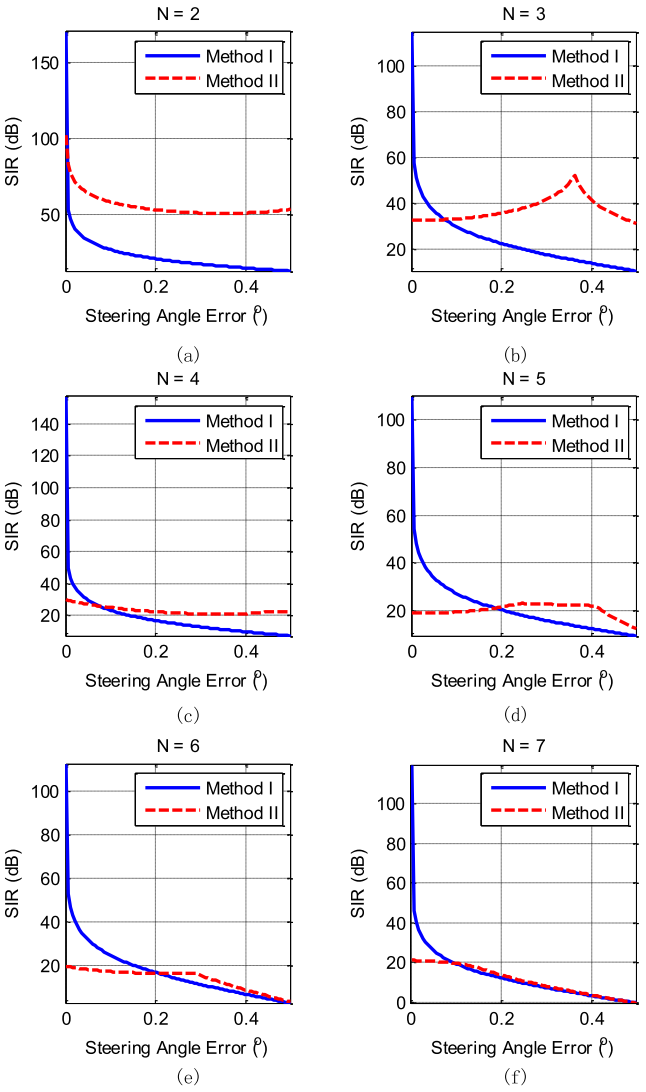

FIGURE 6. SIR vs the steering angle error. (a): $N = 2$. (b): $N = 3$. (c): $N = 4$. (d): $N = 5$. (e): $N = 6$. (f): $N = 7$.

TABLE 2. Parameters used in the system simulation.

f_c	PRF	d	$\Delta\theta$	θ_1	θ_4
10 GHz	500 Hz	0.25 m	2.267 °	86.6 °	93.4 °
T_{pn}	B_{rn}	M	N	$\Delta\tau_2$	SNR
10 μs	750 MHz	8	3	10 μs	0 dB

Even with the increasing of the number of subbeams, there is no obvious deterioration for Method I. The reason is that the optimization solution of Method I forms deep nulls in the directions of the interferences and still maintains the power of the interested target. However, the SIR gets worse with the deviation of the steering angles. For Method II, since it always restricts the sidelobe to a relative low level, it can still achieve a satisfied SIR even if there is a steering angle error. With the increasing of the number of subbeams, the performance of Method II is degenerated. In general, Method I can form deep nulls if there is no steering angle error. Even if there are strong interference targets, Method I can still suppress it. But its performance is decreased with the increasing of steering angle error. Method II can handle the situation with steering angle errors. However, if there is a strong target, for example, the reflectivity of the target is about 20 dB higher than the desired target, Method II cannot effectively suppress it as shown in Fig. 6(d)-(f). In order to solve this problem, more receivers should be utilized.

D. SIGNAL TO NOISE RATIO

The pixel SNR of the MAB ISAR system is investigated at the level of the single-look-complex (SLC) images, compared with that of the equivalent conventional single channel system (short for CON). The equivalent system means one that uses the same pulse duration and energy, peak transmit power, antenna aperture, and monitors the same altitude. The MAB system employs the full area of the antenna aperture to illuminate the wide area with a sequence of narrow and high-gain antenna beams, while the conventional single channel system uses the whole antenna aperture to illuminate the wide area with mandatory expansion of the antenna beam. As a result, the MAB system obtains N times one-way power gain higher than that of the CON system. The receiving gains of the two systems are the same. Therefore, the SNR after signal processing of the MAB system is approximately N times higher than that of the equivalent CON system. It should be kept in mind that the reason for the higher SNR of the MAB system is because of the multiple transmitted pulses, which means that the MAB system consumes more power supply. If the total transmitted power is fixed, the output SNRs would also be the same. However the surveillance velocity range of the MAB system is much larger than that of the CON system.

E. POTENTIAL PROBLEMS

In the discussion above, it is assumed that all the targets are restricted to the corresponding subswaths during the illumination period. However, if there are some targets that have high along-track velocity, they may across the adjacent subswaths. The imaging results will show duplicate targets. To avoid such a problem, the wide subbeams can be adopted. For example, if the slant range from the radar to the target is 10 km, the subbeam width is 6 °, and the along-track velocity of the target is 150 m/s, it will take about 7 s from target to across the subswath, which is much larger than the CPI for high cross-range resolution imaging. In special cases, if the target does across the adjacent subswaths, the images of the same target in different subswaths may be identified by the extracted target features or the auxiliary data obtained by the radar.

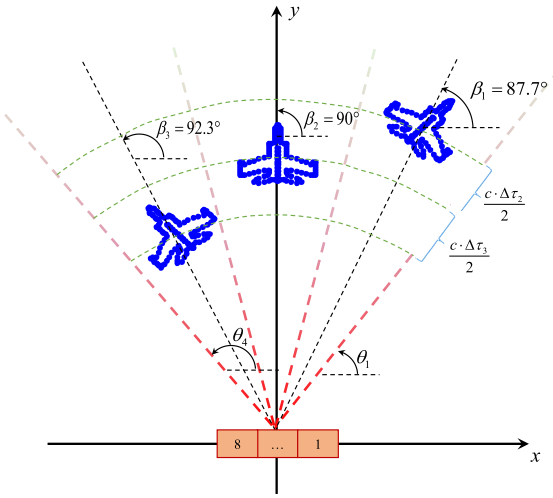

FIGURE 7. Imaging geometry of the designed system.

V. SYSTEM DESIGN AND SIMULATION RESULTS

A. SYSTEM DESIGN

Let us consider an X-band ISAR system located on the ground for air-target surveillance and imaging with the assumption that the required surveillance azimuth angle is about 6.8 °. In order to avoid ambiguities, i.e., grating lobes, in the observation angle range, the distance between adjacent sub-apertures in azimuth should satisfy

$$d \leq \frac{\lambda}{2\sin\theta_{BW}/2}. \tag{26}$$

In this example, d should be less than 0.25 m. Since the whole antenna is used as transmitter and its aperture is divided into equal subapertures as receivers, d is equal to the size of the subaperture. The whole swath is divided into three subswaths. In order to separate the echoes from the subswaths, the number of the subapertures should be greater than three, and therefore, the whole antenna size is at least 0.75 m in azimuth. However, sometimes more receivers are required to improve the system performance, e.g., by achieving higher transmission power. Since the transmitted beamwidth is inversely proportional to the size of the transmitter, the mandatory expansion of the antenna beam is required, which can be

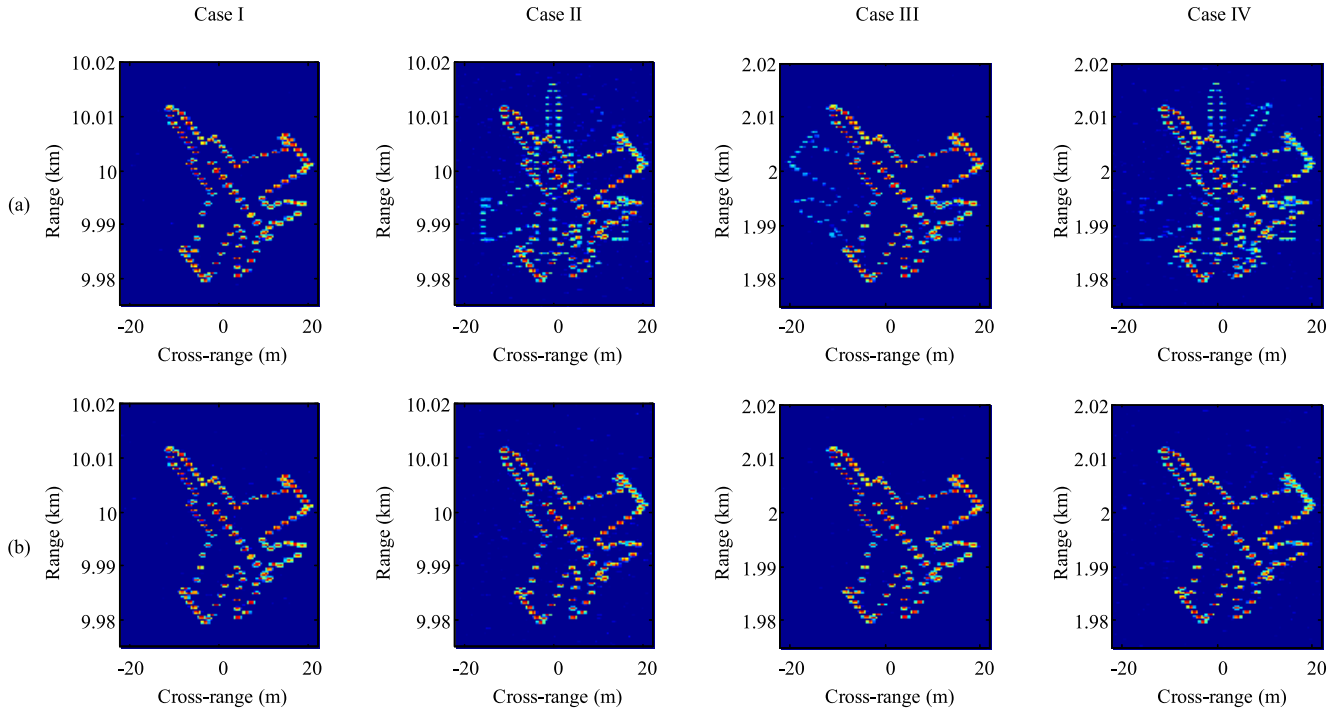

FIGURE 8. Imaging results of Target 3 under different situations by using (a) Method I and (b) Method II, and the four cases are listed in Table 3.

achieved by the spatio temporal modulation of each transmitted radar pulse [23]. In this paper, the whole antenna size is set to be 2 m in azimuth, and divided into eight ($M = 8$) equal subapertures, i.e., each subaperture having a size of 0.25 m in azimuth. The antenna transmits three ($N = 3$) subbeams consecutively in an anti-clockwise direction. The subbeam width is about 2.267 °. Each transmission has a duration of $T_{pn} = 10\ \mu s$, and a bandwidth of $B_{rn} = 750$ MHz to ensure a slant range resolution of 0.2 m. Fig. 7 shows the imaging geometry of the designed system. The surveillance azimuth angle range is from 86.6 ° to 93.4 °, i.e., $\theta_1 = 86.6$ ° and $\theta_4 = 93.4$ °. Three subpulses are steered to azimuth angles $\beta_1 = 87.7$ °, $\beta_2 = 90.0$ °, and $\beta_3 = 92.3$ °, respectively. The system signal to noise ratio (SNR) is set to be 0 dB.

B. SIMULATION RESULTS

In this section, we will use the simulated data to verify the proposed system as well as the processing methods. The simulation parameters are listed in Table 2. The radar center is located at (0 m, 0 m). Without loss of generality, we assume that there are three targets in the surveillance area located in the three subswaths, respectively. The size of all the three targets in azimuth is about 32 m. The center range difference between adjacent targets is about 1.5 km. Since the transmission delay is 10 μs, it is obvious that their echoes reach the receivers simultaneously and therefore are overlapped together in range.

In Fig. 8, the imaging results of Target 3 by using Method I (a) and Method II (b) in terms of four different cases are provided. Limited by length of this paper, the results of the other two targets are not presented, which are similar to that of Target 3. In case I, the slant range of Target 3 to radar is 10 km, and all the targets are located at the center of the subbeams. Case II is the same as Case I except that all the targets are deviated about 0.43 ° from the subbeam center. In case III, the slant range of Target 3 to radar is 2 km, and all the targets are located at the center of the subbeams. Case IV is the same as Case III except that all the targets are deviated about 0.43 ° from the subbeam center. The four cases are summarized in Table 3, where $r_{tr,3}$ represents the slant range from Target 3 to the radar, and $\Delta\alpha$ indicates the deviated angle of the target center from the subbeam center. It should be mentioned that the shorter range implies lower altitude since the grazing angle is fixed. As a comparison, Fig. 9 shows the direct imaging result of one receiver without subpulse separation.

TABLE 3. Four simulation cases: Far range and center, far range and deviated center, near range and center, near range and deviated center.

	Case I	Case II	Case III	Case IV
$r_{tr,3}$	10 km	10 km	2 km	2 km
$\Delta\alpha$	0 °	0.43 °	0 °	0.43 °

In Fig. 8, it can be seen that the target is well focused by both methods in Case I, and no false images of other targets can be observed. When the targets are deviated from the subbeam center in Case II, the signal from other targets cannot be well suppressed by using Method I, and the visible

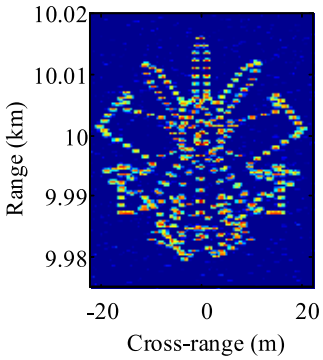

FIGURE 9. Imaging result without subpulse separation.

TABLE 4. ASR of the imaging results.

	Case I	Case II	Case III	Case IV
Method I (dB)	-61.24	-30.57	-45.69	-28.97
Method II (dB)	-58.91	-62.66	-60.01	-58.99

interference components in the final imaging result still exist. The reason is that Method I only restricts the interference signal from the subbeam center. If the interference deviates from the subbeam center, Method I cannot form notch to suppress it. In contrast, Method II can still suppress the signal from other targets in Case II, and the imaging result is clear. The reason is that Method II restricts all the signals coming from outside of the desired subswath rather than forms a deep notch for a certain angle. In Case III, although the targets are located at the subbeam center, their altitudes are much lower resulting in wider angular intervals. For the same reason, Method I cannot suppress the signal coming from outside of the subbeam center, and there are obvious interference components in the imaging results. Method II can still suppress the interference yielding clear imaging result. In Case IV, the similar conclusion can also be drawn.

In order to further illustrate the performance of the proposed algorithms, we use a metric of ambiguity to signal ratio (ASR), which is defined as

$$ASR = \frac{\sum_{(i,j)\in ambiguity} |s_{ij}|^2}{\sum_{(i,j)\in target} |s_{ij}|^2} \tag{27}$$

where s_{ij} represents the (i, j)th pixel of the image. Table 4 gives the ASR of the images corresponding to Fig. 8, which agrees well with the observations. It should be mentioned that for Case I, Method I has achieved a slightly better performance than Method II because Method I forms deep nulls for the interferences exactly.

The computational time in terms of case I is measured based on the MATLAB code run on an Intel 3.2 GHz CPU. Method II is implemented with the CVX toolbox. It turns out that Method I needs 5.09 s and Method II needs 6.14 s.

According to the experiments, it is seen that the proposed MAB ISAR system is able to achieve the wide area multiple moving target surveillance, and both the proposed methods can separate the overlapped signal and obtain high resolution ISAR images. However, Method I has stricter requirement for the system parameters than Method II. Therefore, method I is suitable for higher altitude targets, while method II supports a much wider range of applications. Furthermore, Method I requires that the targets should be located in the direction of the subbeam center, while method II allows much more tolerance on the target position. It should be noticed that since the proposed system is a novel one, there has no real data to confirm the proposed processing methods, and it is difficult to find any existing imaging methods to carry out the comparison.

VI. CONCLUSION

In this paper, a novel wide area MT ISAR imaging system is presented based on multiple azimuth beam and digital beamforming technique. In the proposed system, a large aperture antenna transmits a sequence of narrow and high-gain beams to illuminate a wide area, and all the subapertures receive the echoes simultaneously. To separate the overlapped echoes from different subswaths, two processing methods are proposed based on the beamforming techniques. The experiments show that this novel MAB system has the ability to realize wide area MT imaging. Moreover, it can greatly enlarge the monitorable translational velocity range. Although numerical experimental results manifest the effectiveness of the proposed approach, it is still a conceptual design, and there remains extensive investigations to be carried out to deal with various issues for practical applications.

REFERENCES

[1] V. C. Chen, *Inverse Synthetic Aperture Radar Imaging: Principles, Algorithms and Applications*. Edison, NJ, USA: IET, 2014.
[2] V. C. Chen and Z. Z. Lu, "Radar imaging of multiple moving targets," in *Instrumentation*. San Diego, CA, USA: ISOP, Jul. 1997, pp. 102–112.
[3] S.-H. Park, H.-T. Kim, and K.-T. Kim, "Segmentation of ISAR images of targets moving in formation," *IEEE Trans. Geosci. Remote Sens.*, vol. 48, no. 4, pp. 2099–2108, Apr. 2010.
[4] X. Bai, F. Zhou, M. Xing, and Z. Bao, "A novel method for imaging of group targets moving in a formation," *IEEE Trans. Geosci. Remote Sens.*, vol. 50, no. 1, pp. 221–231, Jan. 2012.
[5] J.-H. Jung, K.-T. Kim, S.-H. Kim, and S.-H. Park, "An efficient ISAR imaging method for multiple targets," *Prog. Electromagn. Res.*, vol. 146, pp. 133–142, Apr. 2014.
[6] Q. Shi, C. Wang, J. Huang, and N. Yuan, "Multiple targets deception jamming against ISAR based on periodic 0-π phase modulation," *IEEE Access*, vol. 6, pp. 3539–3548, 2018.
[7] J. Zhao, M. Zhang, and X. Wang, "ISAR imaging algorithm of multiple targets with complex motions based on the fractional tap length keystone transform," *IEEE Trans. Aerosp. Electron. Syst.*, vol. 54, no. 1, pp. 64–76, Feb. 2018.
[8] S. Gui, J. Li, and Y. Pi, "Security imaging for multi-target screening based on adaptive scene segmentation with terahertz radar," *IEEE Sensors J.*, vol. 19, no. 7, pp. 2675–2684, Apr. 2019.
[9] J. Hao, J. Li, and Y. Pi, "Three-dimensional imaging of terahertz circular SAR with sparse linear array," *Sensors*, vol. 18, no. 8, p. 2477, 2018.
[10] E. Brookner, "Phased-array and radar breakthroughs," in *Proc. IEEE Radar Conf.* Boston, MA, USA: IEEE, Apr. 2007, pp. 37–42.
[11] W. Wiesbeck and L. Sit, "Radar 2020: The future of radar systems," in *Proc. Int. Radar Conf.* Lille, France: IEEE, Oct. 2014, pp. 1–6.
[12] F. Santi, D. Pastina, and P. Lombardo, "ISAR while-scan mode for coastal surveillance," in *Proc. IEEE Radar Conf.* Cincinnati, OH, USA: IEEE, May 2014, pp. 1301–1306.

[13] J. Salzman, D. Akamine, R. Lefevre, and J. C. Kirk, "Interrupted synthetic aperture radar (SAR)," *IEEE Aerosp. Electron. Syst. Mag.*, vol. 17, no. 5, pp. 33–39, May 2002.
[14] L. Zhang, Z.-J. Qiao, M.-D. Xing, J.-L. Sheng, R. Guo, and Z. Bao, "High-resolution ISAR imaging by exploiting sparse apertures," *IEEE Trans. Antennas Propag.*, vol. 60, no. 2, pp. 997–1008, Feb. 2012.
[15] G. Xu, M.-D. Xing, X.-G. Xia, Q.-Q. Chen, L. Zhang, and Z. Bao, "High-resolution inverse synthetic aperture radar imaging and scaling with sparse aperture," *IEEE J. Sel. Topics Appl. Earth Observ. Remote Sens.*, vol. 8, no. 8, pp. 4010–4027, Aug. 2015.
[16] M. Sùss, B. Grafmüller, and R. Zahn, "A novel high resolution, wide swath SAR system," in *Proc. Int. Geosci. Remote Sens. Symp.*, vol. 3, Jul. 2001, pp. 1013–1015.
[17] I. G. Cumming and F. H. Wong, *Digital Processing of Synthetic Aperture Radar Data: Algorithms and Implementation*. Boston, MA, USA: Artech House, 2005.
[18] T. Yang, X. Lv, Y. Wang, and J. Qian, "Study on a novel multiple elevation beam technique for HRWS SAR system," *IEEE J. Sel. Top. Appl. Earth Obs. Remote Sens.*, vol. 8, no. 11, pp. 5030–2039, Feb. 2015.
[19] H. L. Van Trees, *Detection, Estimation, Modulation Theory, Optimum Array Process.*. New York, NY, USA: Wiley, 2004.
[20] M. H. Er, "Array pattern synthesis with a controlled mean-square sidelobe level," *IEEE Trans. Signal Process.*, vol. 40, no. 4, pp. 977–981, Apr. 1992.
[21] S.-X. Zhang *et al.*, "Multichannel HRWS SAR imaging based on range-variant channel calibration and multi-Doppler-direction restriction ambiguity suppression," *IEEE Trans. Geosci. Remote Sens.*, vol. 52, no. 7, pp. 4306–4327, Jul. 2014.
[22] S. Boyd and L. Vandenberghe, *Convex Optimization*. Cambridge, U.K.: Cambridge Univ. Press, 2004.
[23] G. Krieger, N. Gebert, and A. Moreira, "Multidimensional waveform encoding: A new digital beamforming technique for synthetic aperture radar remote sensing," *IEEE Trans. Geosci. Remote Sens.*, vol. 46, no. 1, pp. 31–46, Jan. 2008.

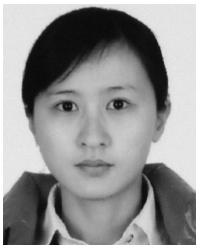

TAOLI YANG (M'16) was born in Leshan, China, in 1987. She received the Ph.D. degree in signal processing from the National Key Laboratory of Radar Signal Processing, Xidian University, China, in 2014. From 2015 to 2016, she was a Postdoctoral Research Fellow with the School of Electrical and Electronic Engineering, Nanyang Technological University, Singapore. She is currently an Associate Professor with the School of Resources and Environment, University of Electronic Science and Technology of China. Her major research interests include SAR/ISAR imaging, interferometric SAR, and ground moving target indication.

LEI YANG (M'15) was born in Tianjin, China, in 1984. He received the B.S. degree in electronic engineering and the Ph.D. degree in signal and information processing from Xidian University, Xi'an, China, in 2007 and 2012, respectively. From 2012 to 2017, he was a full time Research Fellow with the School of EEE, NTU, and a Research Scientist with the Temasek Lab, NTU. He is currently with the Tianjin Key Laboratory for Advanced Signal Processing, Civil Aviation University of China, as an Associate Professor. His main research interests include high-resolution radar imaging and implementation, and sparse Bayesian learning for radar imaging.

GUOAN BI (SM'89) received the B.Sc. degree in radio communications from the Dalian University of Technology, Dalian, China, in 1982, and the M.Sc. degree in telecommunication systems and the Ph.D. degree in electronics systems from Essex University, Colchester, U.K., in 1985 and 1988, respectively. Since 1991, he has been with the School of Electrical and Electronic Engineering, Nanyang Technological University, Singapore. His current research interests include DSP algorithms and hardware structures, and signal processing for various applications, including sonar, radar, and communications.

YONG WANG received the Ph.D. degree from the University of California, Santa Barbara. He is currently with East Carolina University. His research interests include synthetic aperture radar (SAR) and application include the development of SAR imaging algorithm, investigation of scale and scale effect on SAR application to urban target delineation, and evaluation of surface deformation using interferometric SAR (InSAR) techniques.